Catalysis Today 430 (2024) 114536

Contents lists available at ScienceDirect

Catalysis Today

journal homepage: www.elsevier.com/locate/cattod

Photo-Fenton inactivation of MS2 bacteriophage at alkaline pH by Fe salts or nm to μm-sized oxides, and the Janus-faced effects of natural organic matter in surface waters

Na Tian [a,b], Stefanos Giannakis [b,*], Ogadimma Cassandra Oji-Okoro [c], Giulio Farinelli [d], Patricia Garcia-Muñoz [e], Cesar Pulgarin [c,f,g,**]

[a] School of Chemistry and Chemical Engineering, Hunan University of Science and Technology, Xiangtan 411201, PR China
[b] Universidad Politécnica de Madrid, E.T.S. de Ingenieros de Caminos, Canales y Puertos, Departamento de Ingeniería Civil: Hidráulica, Energía y Medio Ambiente, Unidad docente Ingeniería Sanitaria, c/ Profesor Aranguren, s/n, ES-28040 Madrid, Spain
[c] School of Basic Sciences (SB), Institute of Chemical Science and Engineering (ISIC), Group of Advanced Oxidation Processes (GPAO), École Polytechnique Fédérale de Lausanne (EPFL), Station 6, CH-1015 Lausanne, Switzerland
[d] Institut Européen des Membranes, IEM-UMR 5635, Université de Montpellier, ENSCM, CNRS, 34090 Montpellier, France
[e] Department of Industrial Chemical and Environmental Engineering, Escuela Técnica Superior de Ingenieros Industriales, Universidad Politécnica de Madrid, C/ José Gutiérrez Abascal 2, Madrid 28006, Spain
[f] Environmental Remediation and Biocatalysis Group, Institute of Chemistry, Faculty of Exact and Natural Sciences, University of Antioquia, Calle 70 No. 52-21, Medellín, Colombia
[g] Colombian Academy of Exact, Physical and Natural Sciences, Carrera 28 A No., 39A-63 Bogotá, Colombia

ARTICLE INFO

Keywords:
Solar disinfection (SODIS)
virus
photo-Fenton
surface water
nanomaterials
dissolved organic carbon

ABSTRACT

In this study, MS2 bacteriophage was inactivated by homogeneous and heterogeneous photo-Fenton processes in an alkaline matrix (pH 8) using low concentrations of H_2O_2 and iron forms (1 mg/L), including Fe(II), Fe(III), and Fe (hydr)oxides. As a reference, it has been demonstrated that excellent efficiency towards MS2 inactivation was achieved within 2 min with Fe(II) and 10 min with Fe(III) in the homogeneous photo-Fenton process. Mined iron and five naturally occurring iron (hydr)oxides, including wüstite, goethite, hematite, magnetite, and maghemite, were used to assess the virus removal in the heterogeneous photo-Fenton process. Total (5-logU) inactivation of the MS2 bacteriophage was observed within 15–40 min by iron (hydr)oxides in the presence of light and H_2O_2. Photosensitization of natural organic matter had a significant impact on virus inactivation in both homogeneous and heterogeneous photo-Fenton processes, but dually; it enhanced the formation of complexes between organic matter and iron species, facilitating the homogeneous process at alkaline pH, but hindering the heterogeneous photo-Fenton reaction. Nevertheless, the heterogeneous photo-Fenton process may serve as an efficient method for the inactivation of enteric viruses in water, even at a slightly basic pH, despite the scavenging action of natural organic matter. The low-concentration requirements of this process and the availability of iron oxides in nature contribute to the sustainability of the process, which can be suitable for use in resource-poor environments.

1. Introduction

Although approximately 70% of the Earth is covered with water, fresh water suitable for consumption accounts for only 3% of this amount. More than one-seventh of the world's population is compelled to drink untreated water contaminated by human waste and other organic matter [1]. Thus, billions of people still face the risk of suffering from waterborne diseases, such as salmonellosis, typhoid, cholera, and hepatitis A. Hence, research on bacterial- and viral-mediated illness prevention is of fundamental importance.

To ensure that drinking water is safe and free of harmful microorganisms, disinfection is required to inactivate water pathogens including

* Corresponding author.
** Corresponding author at: School of Basic Sciences (SB), Institute of Chemical Science and Engineering (ISIC), Group of Advanced Oxidation Processes (GPAO), École Polytechnique Fédérale de Lausanne (EPFL), Station 6, CH-1015 Lausanne, Switzerland.
E-mail addresses: stefanos.giannakis@upm.es (S. Giannakis), cesar.pulgarin@epfl.ch (C. Pulgarin).

https://doi.org/10.1016/j.cattod.2024.114536
Received 23 November 2023; Received in revised form 7 January 2024; Accepted 16 January 2024
Available online 18 January 2024

protozoa, viruses, and bacteria. Several disinfection methods have been developed over the years, including chlorination, UV radiation, and ozonation [2–8]. Advanced oxidation processes were introduced as an alternative approach for drinking water treatment in the 1980 s, which mostly involved the use of a chemical oxidizing agent combined with UV radiation, a catalyst, or both [9–13]. These processes involve the generation of reactive oxygen species (ROS) that are responsible for the degradation of organic materials and disinfection. Wherein, solar-assisted AOPs have the advantage of using a free, easily accessible energy source and therefore present an ecological alternative to conventional treatment methods [14].

One of the most widely researched photo-assisted AOPs over the last 20 years is the photo-Fenton process [15]. The oxidation of iron in the presence of H_2O_2 produces hydroxyl radicals with high oxidative potential [16,17]. However, if the initial iron form is Fe(III), the reaction kinetics severely decrease. The reduction of ferric ions is several times slower than the initial step and is, therefore, the rate-limiting step of the reaction [18]. In addition, the optimal pH value for the Fenton system is 2.8 [19]. Although ferrous ions are soluble at neutral pH, they precipitate as iron(III) oxyhydroxides if present in the solution [20]. Therefore, in studies dealing with organic contaminant elimination, the main drawback of the homogeneous photo-Fenton reaction is its pH dependence. Another important limitation of Fenton reactions is the production of recalcitrant intermediates such as oxalic acid ($C_2H_2O_4$), which prevents the complete mineralization of organic pollutants [21,22]. Oxalate ions also chelate Fe(III), thereby reducing the Fenton system efficiency. In natural waters, the role of the chelator can be played by the dissolved organic matter derived from natural decomposition processes, transfer of material, or biodegradation.

However, since its discovery, several studies have demonstrated the applicability of photo-Fenton at neutral pH in the inactivation of microorganisms, and the major parameters affecting their efficiency mainly include the reaction temperature, light intensity, concentration of Fenton's reagent, and presence of natural organic matter [23–28]. Since the first works with homogeneous systems (using Fe^{2+} or Fe^{3+} as the starting iron form) [29,30], researchers have investigated more complex forms of facilitating iron, such as iron complexes [20], chelating agents [31,32], and iron oxides [17]. The latter has initiated research owing to the natural availability of iron oxides in nature; hence, their low cost, ease of synthesis under laboratory conditions, and low pH-dependence when applying the photo-Fenton process. The heterogeneous photo-Fenton process is understandably less effective than the homogeneous process at acidic pH, but allows working even at alkaline pH values, constituting an interesting approach for photo-Fenton implementation under field conditions [33]. In addition, natural waters often exceed pH 7, which significantly lowers iron solubility; therefore, a solution to this effect is required. The application of this form of the photo-Fenton process to point-of-use water treatment, especially in developing countries, is potentially feasible owing to the simplicity of the method and its low(er) cost compared to other AOPs [34].

The vast majority of literature on the photo-Fenton process focuses on the removal of bacterial pathogens and significantly less on viruses. However, the severity of the illnesses caused by waterborne viruses requires further investigation. For research purposes on viral vectors, the MS2 bacteriophage, a small (275 Å), icosahedral, RNA virus that infects male *Escherichia coli*, is commonly employed [35]. It is used as a model for enteric viruses because of its comparability in structure and size with several enteric viruses [36]. Its non-pathogenicity in humans, and easy growth and purification under laboratory conditions make it an attractive model for simulating viral pathogens elimination [37–39].

Therefore, filling the literature gaps in water treatment, the efficacy of natural iron oxides, and their use in the photo-Fenton process, the present work investigated the efficacy of homogeneous and heterogeneous photo-Fenton processes on the inactivation of MS2 bacteriophages at alkaline pH. The effect of natural organic matter on virus inactivation during either homogeneous or heterogeneous photo-Fenton processes was assessed. Virus removal based on adsorption in the dark and the photocatalytic properties of the oxides were scrutinized to analyze their contribution to inactivation. Finally, a mechanism was proposed to describe the potential pathways by which MS2 inactivation occurs in the heterogeneous photo-Fenton process.

2. Experimental section

2.1. Chemicals and reagents

All chemicals used to perform experiments in this study were of reagent grade. Solutions were prepared in analytical-grade pure water using a Millipore Elix 3 system coupled to a Prograd filter (Millipore AG, Zug, Switzerland). Natural iron was obtained from an iron mine in Colombia (Duitama, Boyacá), wüstite, goethite, maghemite, nano-maghemite, magnetite, and nano-magnetite were purchased from Sigma-Aldrich, while hematite was purchased from ABCR and nano-hematite from Alfa-Aesar. Ferrous sulfate heptahydrate ($FeSO_4 \bullet 7 H_2O$) and ferric sulfate ($Fe_2(SO_4)_3$) were used to prepare Fe(II) and Fe (III) solutions, respectively. Iron salts and hydrogen peroxide (H_2O_2) were obtained from Sigma-Aldrich. The classification and properties of various iron species are summarized in Table S1 (Supporting Information, SI). The related natural organic matter stock solution and water matrix are provided in Test S1 in the SI.

2.2. Microorganisms and cultivation methods

2.2.1. MS2 bacteriophage and bacterial host

The viral model MS2 bacteriophage (DSMZ 13767) and its *Escherichia coli* (*E. coli*) host (DSMZ 5695) were obtained from Deutsche Sammlung von Mikroorganismen and Zellkulturen (DSMZ, Braunschweig, Germany). Phage purification and propagation were performed according to the protocol described by Ortega-Gómez et al. [40]. Solutions for viral and bacterial cultivation are presented in Supplementary Text S2.

2.2.2. Phage quantification

The concentration of infective MS2 was measured by the double-layer agar method and expressed as plaque-forming units (PFU/mL). The Petri dishes were placed for 24 h in an incubator (B 5060 EK-CO_2, Heraeus Instruments, Hanau, Germany) under controlled temperature levels (37°C). The detection limit of this method was 10 PFU/mL.

2.3. Inactivation experiments and data analysis

All experiments were performed using a Suntest CPS solar simulator with a radiation intensity of 900 W/m^2 in UV-B transparent glass reactors containing magnetic bars with constant agitation at 350 rpm. All details are presented in Supplementary Text S3. At the beginning of each experiment, reactors containing 100 mL of virus-suspended carbonate-buffered saline were stirred in the dark for 15 min to achieve even distribution. The initial concentration of MS2 was approximately 10^6 PFU/mL for the first set of experiments performed to test the effect of different TOC levels of natural organic matter (NOM) and recreate the results of the homogeneous photo-Fenton process and the individual reactions of its constituents with light. All further experiments were performed at an initial concentration of 10^5 PFU/mL. The reactors were spiked with freshly prepared iron solution (1 mg/L), according to the conditions of each experiment. A similar concentration of H_2O_2 was added after the catalyst in the Fenton or photo-Fenton reaction. The choice of reagents' addition was performed following Ortega-Gómez et al. [40]; higher concentrations may confound the inactivation tests, diminish the differences in the various constituents, and add important influence from other mechanisms (e.g., adsorption). The samples were exposed for 60–120 min under simulated sunlight.

During the experiments, 100 μL samples were collected and immediately diluted in 900 μL CBS, where they remained stable. Subsequently, 10-fold serial dilutions were performed, depending on the experiment. The experiments were performed in duplicate (minimum) and the results were plotted as PFU/mL over time. MS2 bacteriophage titers were calculated using the arithmetic mean of the last two serial sample dilutions ± standard deviation. The observed k (k_{obs}) was obtained using linear regression between $\ln([virus]_0/[virus])$ and time, and the surface-normalized inactivation rate k^1_{obs} was calculated by dividing k_{obs} by the oxide-specific surface area.

2.4. UV titration method

The equivalence point between the central ion and a slightly basic aqueous solution of NOM (50 mg/L) was determined using UV titration. UV titration was performed by gradually increasing the amount of iron in a solution of NOM 50 mg/L and taking the spectrum after each addition of iron.

3. Results and discussion

3.1. MS2 bacteriophage inactivation by the constituents of the photo-Fenton process (Fe, H_2O_2, and light) and their combination

First, several experiments were performed to assess the individual effects of solar irradiance alone, as well as the Fenton reaction constituents, i.e., hydrogen peroxide, and iron species (Fe^{2+} and Fe^{3+}) under solar light on viral inactivation. Classical homogeneous photo-Fenton reactions occurred in these systems, and the obtained results could be used to further guide and analyze the effect of natural organic matter on the photo-Fenton reactions. As depicted in Fig. 1a, it could be observed that the inactivation of MS2 was negligible (< 0.5 log) under solar irradiation (900 W/m^2) for 120 min. This provides evidence for the high resistance of the MS2 phage to UV radiation, corresponding to results from previous experiments [40,41]. Its high cytosine and guanine content could play a role in UV resistance, since the main pathway of UV damage is thymine (and, to a lesser extent, cytosine) dimers [42].

Complete inactivation of MS2 was observed within 60 min of the addition of 1 mg/L H_2O_2 under solar irradiance with the same power density (hereafter, complete or total inactivation refers to the decrease to, or below, the detection limit, shown in figures as DL). Since solar light alone did not lead to significant inactivation and there was no obvious inactivation of MS2 in previous studies when H_2O_2 was added to MS2 samples in the absence of light [43], it can be interpreted that there was a combined action of H_2O_2 and solar light on the viruses. Solar radiation likely increases the sensitivity of MS2 phage, making it more vulnerable to the oxidative action of H_2O_2, thereby enhancing inactivation. Hydrogen peroxide undergoes poor photolysis, which supports our previous hypothesis.

Similarly, complete inactivation was achieved within 60 min with 1 mg/L Fe^{2+} and Fe^{3+} under solar exposure (brown and red lines in Fig. 1a). Dissolved Fe(II) decreased virus concentration faster than that with Fe (III), but both dissolved iron species achieved faster inactivation than the solar/H_2O_2 system. The difference in kinetics observed between the two iron species suggests that ferrous ions undergo a rapid reaction at the initial stage, which leads to the inactivation of more viruses and their conversion to ferric ions. Subsequently, both the iron species continued the catalytic cycle. Electron transfer from Fe probably occurred in the initial phase by reducing the capsid elements of the virus with the oxidation of Fe(II) to Fe(III). The addition of hydrogen peroxide to the iron/light systems significantly accelerated MS2 inactivation, and the detection limit was reached within 2 min for ferrous ions and 10 min for ferric ions. This indicates that the photo-Fenton reaction is suitable for MS2 inactivation in water. The first phase was most likely influenced by the Fenton process (Eq. 1) and the second phase of inactivation, which is governed by the light-assisted conversion of ferric ions back into ferrous ions (Eq. 2) occurred after the first two minutes. Higher reagent concentrations may enhance the first phase of inactivation, whereas the concentrations chosen in this study mitigated this effect.

$$Fe^{2+} + H_2O_2 \rightarrow Fe^{3+} + OH^- + HO^\bullet \; k = 76\ M^{-1}\ s^{-1} \quad (1)$$

$$Fe^{3+} + H_2O_2 \rightarrow Fe^{2+} + H^+ + HO_2^\bullet \; k = 1\bullet10^{-3}\ M^{-1}\ s^{-1} \quad (2)$$

3.2. MS2 bacteriophage inactivation by photosensitization of natural organic matter

Photoinactivation of microorganisms can occur either by light-mediated damage to cells or indirectly through the production of reactive species by photosensitizers. To assess the efficiency of indirect photo-inactivation on MS2, two types of sensitizers, Suwanee River Natural Organic Matter (SRNOM) and Nordic Lake Natural Organic Matter (NLNOM), were added to MS2 samples at different TOC levels (1, 2, 5, 10 mg/L) and exposed to solar light for 2 h. Fig. S1 shows that MS2 is more efficiently inactivated with an increase in organic carbon content. It was reported that at low aromatic carbon contents, the reactive species responsible for inactivation of the MS2 bacteriophage were $^1O_2$

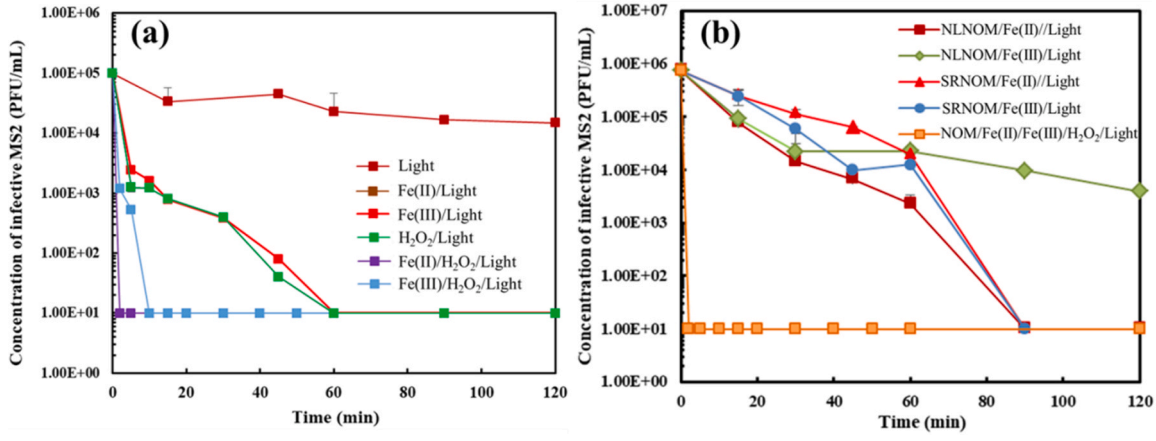

Fig. 1. (a) Individual effects of solar irradiance (900 W/m^2) and combined effects of Fe^{2+}/Fe^{3+} (1 mg/L), H_2O_2 (1 mg/L), and both Fe^{2+}/Fe^{3+} and H_2O_2 on MS2 bacteriophage inactivation. Note: Fe(II)/Light (brown trace) and Fe(II)/H_2O_2/Light (purple trace) have identical profiles (i.e., overlapping traces). (b) Inactivation curves of MS2 by different photoreaction systems in the presence of Fe(II)/Fe(III) (1 mg/L), light (900 W/m^2), and (NL or SR) NOM (TOC = 1 mg/L. Note: The orange trace refers to either type of NOM and/or Fe ions).

and the triplet excited state of dissolved organic matter, ^{3}DOM* [44]. As shown in Fig. S1, the presence of NLNOM greatly enhanced MS2 photoinactivation, even at low TOC values. In particular, a decrease of 1.62 log was observed with 1 mg/L TOC. Inactivation increased with an increase in the amount of TOC, and the detection limit was reached within 90 min at a TOC concentration of 10 mg/L. SRNOM also enhanced MS2 inactivation with a decrease of 0.7 log at 1 mg/L TOC after 2 h under light and 2.52 log when TOC was increased to 10 mg/L. In addition to the singlet oxygen and triplet states of organic matter, other reactive species generated in the presence of photosensitizers present in NOM include hydroxyl radicals, hydrogen peroxide, and superoxide [28]. However, a further increase in the concentration of natural organic matter may reduce the efficacy of inactivation by self-scavenging reactive species. To maintain realistic and environmentally relevant NOM concentrations, all tests with NOM were performed with 1 mg/L TOC content.

The results clearly demonstrate that more reactive species are generated upon irradiation with NLNOM than with SRNOM, which can be attributed to the difference in the composition of the organic matter. As previously reported, the free radical generation potential of humic substances depends on the H:C ratio. Humic acids (HA), which have a lower H:C ratio than fulvic acids, lead to higher free radical production [45]. As a result, it can be expected that between the two NOM sources used in this experiment, the one with the higher concentration of HA would initiate the generation of more reactive species, that is, NLNOM, rather than SRNOM.

Although the ability of NOM to coordinate iron ions is known, the stoichiometry of the interaction between certain NOM and iron ions has not yet been quantitatively tested. To determine the NOM-metal binding stoichiometry, which is the ratio between the concentration of NOM (mg/L) and the concentration of the central ion (mM), UV titrations were performed with Fe(II) and Fe(III) as the catalytic core, and NLNOM and SRNOM as complexing agents. Table 1 reports the concentration of the various NOM associated with each equivalence point with the central ion, that is, the inflection point of the titration curve, in a slightly basic aqueous solution of NOM (50 mg/L) (see Fig. S2 in the SI) Supporting Information for the titration curves). The formation of proper complexes appeared to occur with Fe(III) and NLNOM-Fe(II). The lower affinity of NOM to Fe(II) is most likely related to two major reasons: geometry and electronics. The first is the higher atomic ray of Fe(II) compared to Fe(III), which is more difficult to complex from a highly condensed molecular structure with a low H:C ratio, and hence low flexibility, as NOM is. The second is due to the lower charge of Fe(II), which allows weaker electrostatic interactions compared to Fe(III).

From Table 1, it is evident that SRNOM has a higher affinity for Fe (III) than NLNOM does. Indeed, a higher affinity for iron ions implies lower accessibility of the metal as the catalyst, resulting in a lower inactivation efficiency. In addition, the weaker interaction between NOM and Fe(II) further explains and corroborates the higher efficiency of the Fe(II) systems. Indeed, the complexing ability of NOM plays an antithetical role both in the homogeneous presence of iron ions in slightly basic media and in lowering their accessibility as a catalyst during inactivation. Overall, the measured equivalence point is mainly employed to understand the ability of the target NOM to interact with metals and to correlate this data with the inactivation ability of the systems.

Table 1
Metal concentration at saturation (equivalence point) in NOM-iron ion complexes at a NOM concentration of 50 mg/L.

Complexing agent (50 mg/L)	Central ion	Equivalence point
NLNOM	Fe(II)	~8.5 mM
NLNOM	Fe(III)	~9.5 mM
SRNOM	Fe(III)	~17 mM

3.3. Effect of NOM on MS2 bacteriophage inactivation by Fe/light and photo-Fenton systems

To assess the effect of these organic compounds on the photo-Fenton reaction, several experiments were performed with both ferrous and ferric iron in the presence of light and NOM. Compared with the results obtained in the absence of NOM (Fig. 1a), the inactivation efficiency of the Fe/light systems decreased in the presence of both NLNOM and SRNOM (Fig. 1b), demonstrating the chelating effects of NOM. Nevertheless, in 90 min, ferric ions yielded a 4-log inactivation with NLNOM, whereas the other experiments achieved total inactivation.

Photo-Fenton reactions with ferrous ions achieved total inactivation in the same 2-min period as in the absence of NOM. In addition, the inactivation time decreased from 10 to 2 min in the case of ferric ions, which probably shows that with Fe^{2+}, the reaction could be faster (but impossible to measure with conventional plating). The above results also showed that although NOM affected the efficiency of inactivation with the Fe/light systems, a significant enhancement of MS2 inactivation was observed in the presence of NOM by photo-Fenton reactions (Fig. 1b). This was attributed to the formation of Fe-organic complexes that i) maintained iron in the solution for a longer time in this alkaline environment and ii) exhibited photocatalytic properties, exploiting the chelating effects of the ligands. Upon irradiation, electron transfer occurred from the ligand to the ferric ion, producing organic radicals and ferrous ions. The generation of an additional ferrous ion, which produces hydroxyl radicals in the presence of H_2O_2, accelerates the photo-Fenton process in the presence of NOM.

3.4. Comparison of MS2 bacteriophage inactivation by homogeneous Fenton(-like) and heterogeneous photo-Fenton reactions

In nature, iron is commonly found in the form of oxides. Ferrous ions undergo spontaneous oxidation by oxygen and are transformed into ferric ions (Eq. 3). The process involves partially oxidized metastable intermediate species that are finally converted to stable iron oxides, including lepidocrocite, magnetite, goethite, and hematite. The nature of the oxides formed depends on the oxidation rate, pH, and solution composition [46]. Hence, to assess the efficiency of iron oxide-mediated inactivation of MS2 bacteriophages, 1 mg/L Fe(II) and Fe(III) solutions were prepared and aged for different time intervals (4 h, 24 h, 48 h, and 1 week) to initiate the generation of oxides.

$$4Fe^{2+}_{(aq)} + O_{2(g)} + 4\ H^{+}_{(aq)} \leftrightarrow 4Fe^{3+}_{(aq)} + 2\ H_2O_{(l)} \quad (3)$$

In our experiments, having Fe(II) as a starting iron source, at 25 °C and normal O_2 concentrations, oxidation to $Fe(OH)_x^{3-x}$ or $Fe(OH)_y^{2-y}$ occurs, leading to:

i) Green rusts via precipitation, followed by further oxidation to lepidocrocite (for our solution at near-neutral pH), and after dehydroxylation to maghemite, or
ii) Magnetite (and maghemite) can also be the final product of the oxidation and dehydration of hydroxyl complexes.

Starting with Fe(III), oxidation to $Fe(OH)_x^{3-x}$ takes place, leading to:

a) Goethite, or
b) Ferrihydrite, and then hematite

In the presence of light only, that is, oxidized Fe/sunlight, total inactivation was achieved with all ferrous ion-originating stock solutions within 60–90 min, as shown in Fig. 2a. The corresponding ferric compounds were also very efficient for MS2 inactivation, and more than 3 log reductions were obtained after 2 h. The addition of H_2O_2 accelerated the decrease in phage titration counts and achieved total inactivation in 10 min (Fig. 2b), demonstrating the efficacy of naturally

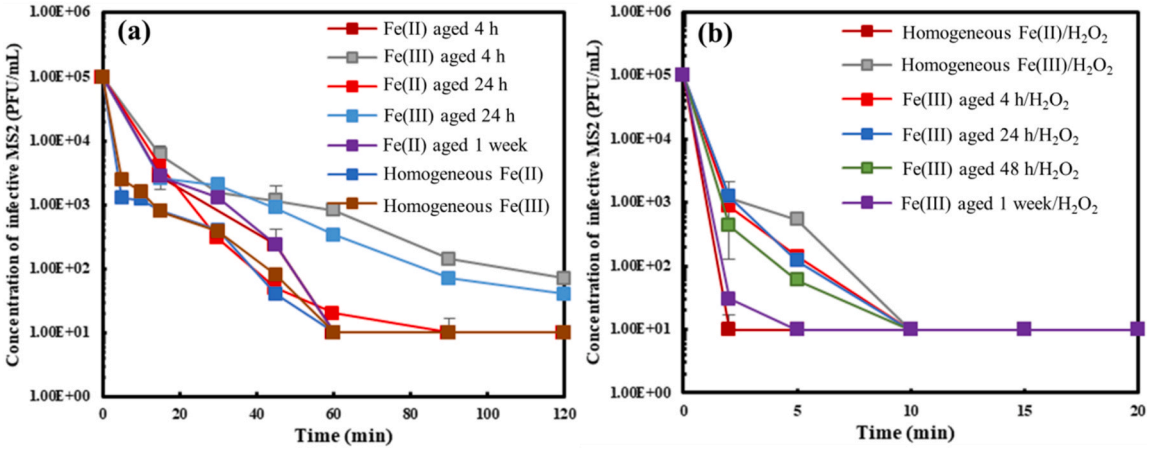

Fig. 2. MS2 bacteriophage inactivation by (a) light-assisted process with Fe(II), Fe(III), or *in-situ* generated iron oxides and (b) homogeneous and heterogeneous photo-Fenton (900 W/m^2, [Fe(II), Fe(III), iron oxides]= 1 mg/L, [H_2O_2] = 1 mg/L).

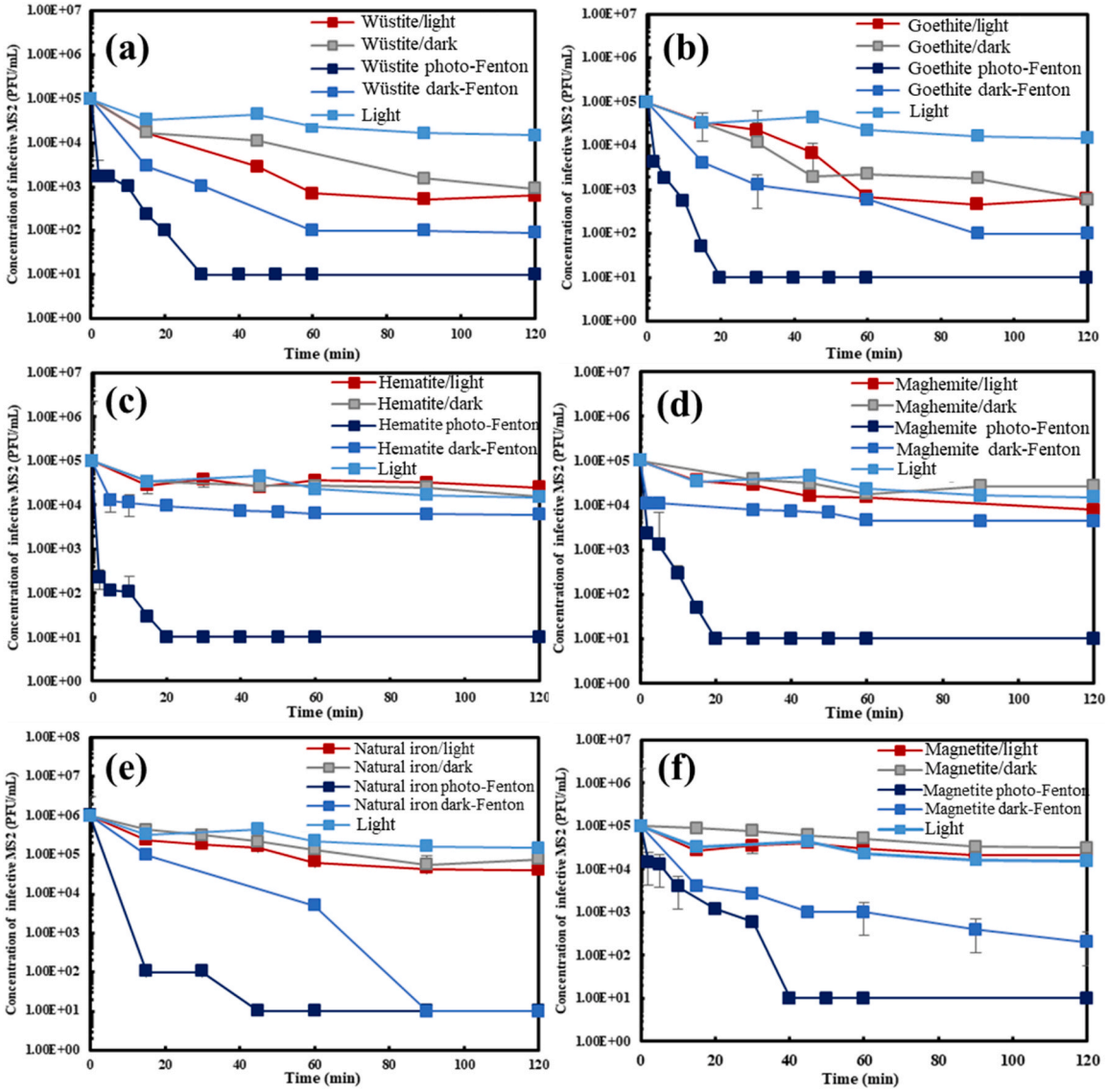

Fig. 3. MS2 bacteriophage inactivation by iron (hydr)oxide particles in the presence or absence of light, light-assisted reactions with H_2O_2, and oxides with H_2O_2 for (a) wüstite, (b) goethite, (c) hematite, (d) maghemite, (e) natural iron, and (f) magnetite (900 W/m^2, [iron oxide] = 1 mg/L, [H_2O_2] =1 mg/L).

generated iron oxides in the oxidized-Fe/light and photo-Fenton(-like) inactivation of MS2. Therefore, further experiments were conducted to assess the efficacy of iron oxides in the controlled heterogeneous photo-Fenton process.

Five commercial oxides and iron from a mine were tested for their potential to act as Fenton catalysts. To define the individual processes contributing to the heterogeneous photo-Fenton reaction, virus-oxide interactions in the dark (adsorption), photocatalytic semiconductor action in the presence of light, heterogeneous Fenton, and heterogeneous photo-Fenton processes were performed. From Figs. 3a and 3b, it was observed that wüstite and goethite demonstrated a decrease in phage titers in the dark, leading to a 2-log reduction, whereas the remaining oxides achieved less than 1 log reduction. Virus-oxide interactions are influenced by the isoelectric point (IEP) of the oxides as well as the size of the particles. Wüstite and goethite favor adsorption at neutral pH because they present a positive charge in this solution, promoting their interaction with negatively charged virions. In presence of light, wüstite and goethite achieved significant additional inactivation, exhibiting semiconductor photocatalytic properties, since their v_B potential, 2.93 and 2.23 eV are higher than the potential of $H_2O/^{\bullet}OH$ pair (1.98 eV) [17]. For both oxides, it can be observed that, initially, the reaction proceeds at the same rate as in the dark before acceleration occurs. This demonstrates that virus-oxide interaction (adsorption) occurs first or has a more dominant effect, followed by the semiconductor effects of solar irradiation. For the rest of the oxides (Fig. 3c-f), irradiation enhanced inactivation only slightly compared to that achieved in the dark, which demonstrated that the semiconductor action did not play a significant role in disinfection of the CBS matrix, which can be explained by the following aspects:

1) Oxides with similar v_B energies are negatively affected by smaller specific surface areas (e.g., hematite vs. goethite)
2) Similar oxide composition but different crystalline structures can have an effect (e.g., maghemite γ-Fe_2O_3 vs. hematite α-Fe_2O_3)
3) The CBS matrix contains carbonate, which can compete with photogenerated h^+ and •OH in solution.

Upon addition of hydrogen peroxide in the dark, wüstite and goethite achieved an additional 1 log reduction, whereas inactivation with maghemite and hematite was not significantly enhanced. However, magnetite and natural iron exhibited excellent performance with H_2O_2, achieving total inactivation in 90 min and 4-log reduction after 2 h with magnetite, as shown in Figs. 3e and 3f. The acceleration observed with magnetite in this system can be attributed to its composition. As a ferrous-ferric oxide, magnetite is a direct Fe^{2+} source that catalyzes the Fenton reaction. The XRF analysis showed that the iron used in this study had an iron content of 81.26%. Its performance in this system could also be related to the high iron content of the solution, as this natural iron was observed to be highly soluble. In the dark, iron oxides can react directly with hydrogen peroxide to generate ferric ions and hydroperoxyl radicals, which can undergo a reversible reaction to produce singlet oxygen (Eqs. 4–6).

$$>Fe^{3+}OH + H_2O_2 \rightarrow >Fe^{2+} + HO_2^{\bullet} + H_2O \quad (4)$$

$$HO_2^{\bullet} \leftrightarrow O_2^{\bullet-} + H^+, pK_a = 4{\cdot}8 \quad (5)$$

$$h_{vb}^+ + O_2^{\bullet-} \rightarrow {}^1O_2 \quad (6)$$

$$>Fe^{3+}OH + h\nu \rightarrow >Fe^{2+} + \bullet OH \quad (7)$$

$$>Fe^{2+} + H_2O_2 \rightarrow >Fe^{3+} + \bullet OH + OH^- \quad (8)$$

$$>Fe^{3+}OH + HO_2^{\bullet}/O_2^{\bullet-} \rightarrow >Fe^{2+} + H_2O/OH^- + O_2 \quad (9)$$

The addition of 1 mg/L H_2O_2 to the iron oxide/light system accelerated viral inactivation, and the detection limit was reached for all oxides in less than 60 min. The reactions occurring in the presence of both iron oxides and hydrogen peroxide are described by Eqs. 4–9. Iron oxides are photo-reduced to ferrous ions and hydroxyl radicals (Eq. 7), and an additional hydroxyl radical is produced by the reaction between ferrous ions and H_2O_2 (Eq. 8). Hence, the efficiency of the heterogeneous photo-Fenton process can be attributed to the production of reactive species near adsorbed viruses. Another mechanism that occurs upon irradiation of iron oxides at neutral pH was proposed, that is, $>Fe^{4+}=O$, and a hydroxyl radical was generated in the photo-reduction of iron oxides (Eq. 10). Moreover, the reaction of $> Fe^{4+}=O$ with water formed an additional hydroxyl radical (Eq. 11), which can also exert a direct oxidative action on the viral capsid.

$$>Fe^{3+}\text{-}OOH + h\nu \rightarrow >Fe^{4+}=O + \bullet OH \quad (10)$$

$$>Fe^{4+}=O + H_2O \rightarrow >Fe^{3+}\text{-}OH + \bullet OH \quad (11)$$

In addition, we mentioned before that the particle size of iron oxides may affect the inactivation efficiency of MS2 bacteriophages during heterogeneous photo-Fenton processes. Hence, the inactivation of MS2 in the presence of several iron oxides and their nanosized equivalents was compared in light-only and heterogeneous photo-Fenton processes to investigate the influence of the particle size on the efficiency of iron oxides and their nano-counterparts. Fig. 4a shows that the size of the iron oxide particles did not influence virus inactivation in the semiconductor reaction (light only). However, as shown in Fig. 4b, photo-Fenton disinfection with nanosized iron oxides (both maghemite and hematite) was slower than disinfection with the original oxides in the photo-Fenton experiments. This phenomenon could be attributed to the difference in efficiency per square meter between iron oxides and nanosized oxides. Because adsorption is a crucial first step, more viruses would adsorb to micrometer-sized oxides than to oxides on the same nanoscale as MS2 and would possibly undergo a higher number of oxidation reactions.

The observed first-order inactivation rate k_{obs} was calculated for the heterogeneous photo-Fenton processes based on the slope of the linear regression between $\ln([virus]_0/[virus])$ and time [47]. Surface-normalized inactivation rates k_{obs}^l were also calculated for some oxides as a function of the surface area (a, m^2/g) (Eq. 12). From Table 2, it can be observed that the surface-normalized inactivation rate constants of the nanosized oxides are approximately ten times less than their iron oxide equivalents. Iron oxides are approximately 5 μm in size and, therefore, have a higher efficiency per area than nanosized oxides on viruses (27.5 nm).

$$k_{obs}^l = k_{obs} \text{ x } (a)^{-1} \quad (12)$$

However, if an application is intended to be performed, cost-effectiveness (efficiency) is always a factor in the selection of a catalyst (Eq.13). In Table 2, the cost for 1 g of oxide and the price necessary to inactivate 1 cell per min is presented. Although goethite presented the fastest k_{obs}, the most efficient catalysts were hematite, maghemite, and magnetite. The availability of mass production methods makes them more competitive than other oxides that generally perform better (e.g., wüstite) or their nano-equivalents.

$$\text{Unitary cost} = k_{obs} \text{ / Cost} \quad (13)$$

3.5. Effect of NOM on MS2 bacteriophage inactivation by heterogeneous photo-Fenton reactions

Humic acids have an isoelectric point (IEP) of 2, whereas the MS2 bacteriophage has an IEP of 3.9 [17,48]. Therefore, the negatively charged organic compounds compete with virus particles for iron active sites (positively charged), reducing the available surface area for virus-oxide interactions. Hence, the presence of natural organic matter one would expect to negatively affect the efficiency of iron oxides. In the

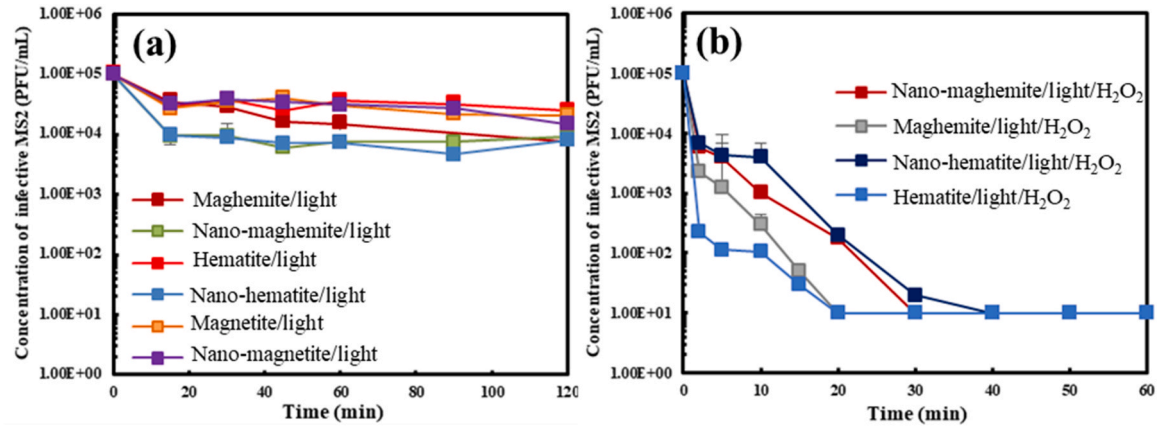

Fig. 4. Influence of oxide size on MS2 bacteriophage inactivation in the presence of (a) light (900 W/m^2), and (b) light and H_2O_2 (900 W/m^2 and 1 mg/L).

Table 2
Kinetics of MS2 inactivation by heterogeneous photo-Fenton processes at neutral pH. Underlined bold indicates the most effective process, underlined the 2nd, and underlined italics the 3rd most effective process.

Iron (hydr)oxide	Inactivation rate constant, k_{obs} (cells/min^{-1})	Surface area, **a** (m^2/g)	Surface-normalized rate constant, k^I_{obs} (g/min.m^2)	Cost for 1 g oxide (€)	Unitary cost k_{obs}/Cost (cells/€.min)
Wüstite	0.2461	10	0.0246	10.92	0.0023
Goethite	**0.4081**	37	0.0110	0.80	0.0137
Hematite	*0.3275*	5.8	0.0564	0.07	**0.7601**
Maghemite	0.3923	5.3	**0.0740**	0.13	0.5572
Magnetite	0.1866	6.5	*0.0287*	1.39	*0.0206*
Nano-magnetite	0.2722	40.8	0.0067	1.69	0.0040
Nano-maghemite	0.2612	31.02	0.0084	6.32	0.0013
Natural iron	0.2301	14.01	0.0164		

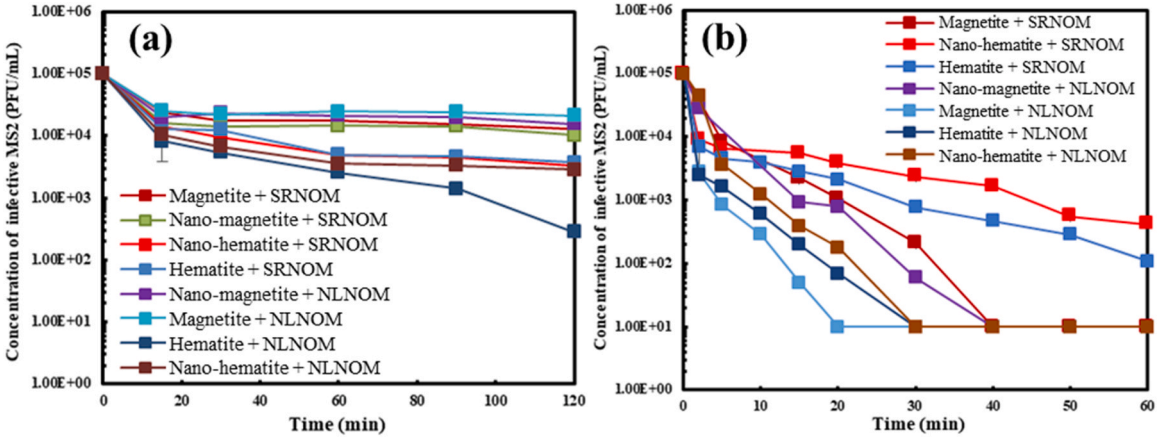

Fig. 5. MS2 bacteriophage inactivation with iron (hydr)oxide particles in the presence of NOM and (a) light (900 W/m^2) and (b) Light and H_2O_2 (900 W/m^2 and 1 mg/L).

presence of H_2O_2, the reactive species produced in Fenton-like processes are scavenged by NOM, reducing the kinetics of the reaction. Fig. 5a shows that except for the mild effect of NLNOM on hematite, the presence of NOM did not influence the reaction with iron oxides in the presence of light, as compared to Fig. 4a.

However, the heterogeneous photo-Fenton processes were similar or less effective than those in the absence of NOM (Fig. 5b). NOM scavenges hydroxyl radicals, reducing the efficiency of iron oxides in the heterogeneous photo-Fenton process (except Magnetite + NLNOM). Despite the negative action of NOM on the iron oxide catalyst, the detection limit was reached for most oxides in less than an hour demonstrating the efficiency of this process in presence of chelating agents naturally present in surface and underground waters.

3.6. Mechanism of MS2 bacteriophage inactivation by heterogeneous photo-Fenton processes

Based on the experimental results and a critical review of the literature, a mechanistic interpretation of the pathways contributing to MS2 inactivation by homogeneous and heterogeneous photo-Fenton processes is proposed and illustrated in Fig. 6.

Firstly, starting from the inside out, upon exposure to solar light in pathway 1 damage to nucleic acids moderately affects MS2 bacteriophage infectivity [49]. UV light also causes protein damage [50].

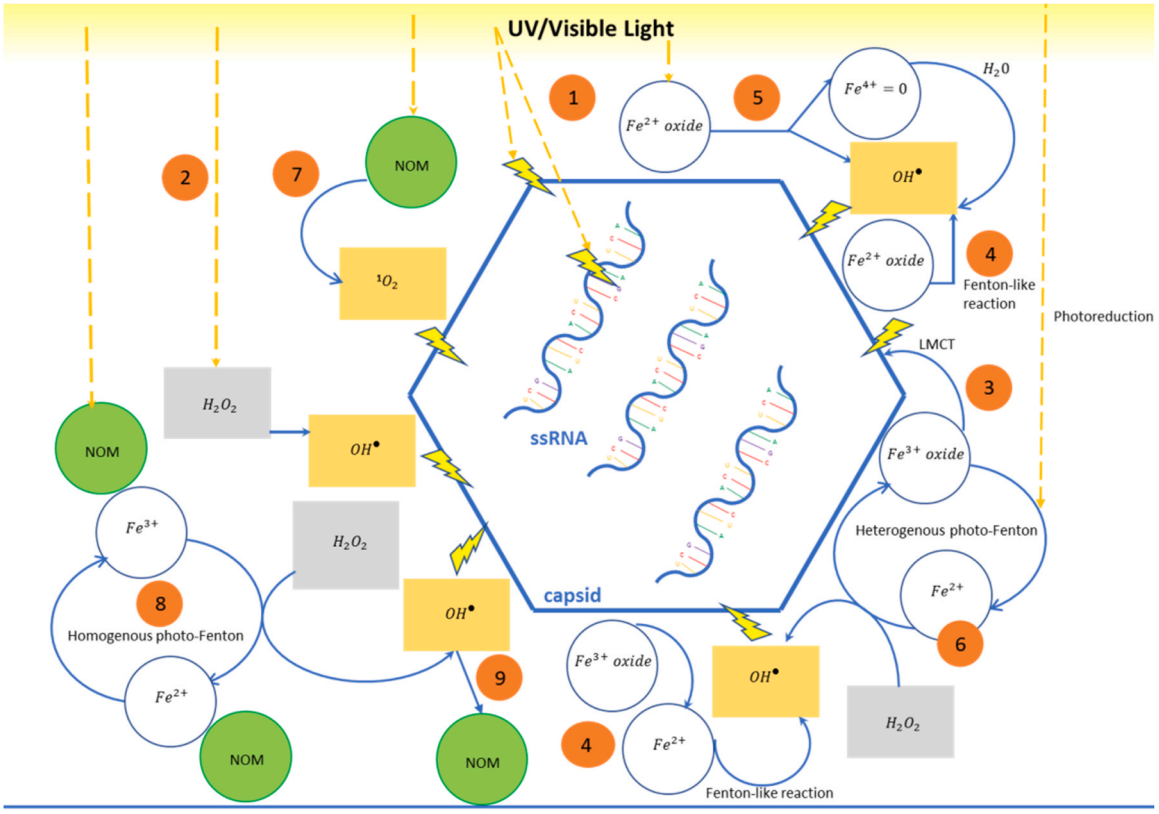

Fig. 6. Integrated proposal of the pathways leading to MS2 bacteriophage inactivation by homogeneous and heterogeneous photo-Fenton processes.

However, these processes do not appear to play key roles in the loss of viral infectivity.

As depicted in pathway 2, H_2O_2 exerts oxidative stress on MS2 bacteriophages, interfering with viral repair mechanisms that aid in the repair of UV-mediated genomic and protein coat damage [40]. In addition, physical adsorption onto iron oxides enhances the removal of viruses from water [51]. This is a result of the electrostatic interactions between positively charged iron oxides and MS2 particles, which are negatively charged and have an isoelectric point of 3.9 at neutral pH [52]. Fe^{3+} serves as an electron acceptor for LMCT with viral capsid proteins in pathway 3.

In absence of light, iron (II) oxides react immediately with H_2O_2 to initiate the Fenton process, as shown in pathway 4. However, iron (III) oxides are reduced by H_2O_2, generating hydroperoxyl radicals and ferrous ions that initiate the Fenton reaction [53]. Hydroperoxyl radicals can undergo reversible reactions to produce singlet-oxygen species. The interaction of ferrous ions with the viral capsid allows Fenton reactions to occur on the viral surface [43].

When light is provided to the system, iron oxides undergo a photoreduction process to produce hydroxyl radicals and ferrous ions in the presence of light, as shown in pathway 5. In addition, the photodissolution of iron oxides also yields Fe(IV) species, which can react with water to generate hydroxyl radicals.

In the simultaneous presence of light and H_2O_2, the photo-generated ferrous ions undergo a homogeneous photo-Fenton reaction, producing an additional hydroxyl radical (pathway 6). In presence of light, ROS are generated within NOM macromolecules, with the predominant species in the system being $^1O_2$ [54]. Complexation of NOM with virus particles and iron oxides allows the production of ROS near the virus, thereby enhancing inactivation in pathway 7.

Finally, the photoactive Fe(III)-organic complexes undergo a homogeneous photo-Fenton reaction in the presence of H_2O_2, producing hydroxyl radicals in pathway 8. However, organic matter competes with viruses for active sites on the oxides and scavenges ROS (pathway 9).

4. Conclusions

As suggested by the experimental data of this work, the homogeneous and heterogeneous photo-Fenton process as a means of MS2 bacteriophage elimination method is effectively applied under slightly basic conditions and in the presence of carbonates, assisted by the presence of NOM. Following the synthesis of the experimental data from this work and the body of literature on the topic, an integral mechanism of MS2 bacteriophage inactivation is provided.

Solar light-assisted reactions with Fe(II) and Fe(III) salts as the initial iron forms were very efficient against virus infectivity, even in the absence of H_2O_2, achieving total inactivation within 1 h. The results of photo-sensitization of NLNOM and SRNOM demonstrated the influence of exogenous ROS generated in sunlit waters on the inactivation of viruses. The complexation of these organic compounds with ferrous or ferric iron enhances their solubility at neutral and basic pH and promotes LMCT reactions with the capacity to inactivate MS2 bacteriophage. We report that NOM enhanced the homogeneous photo-Fenton process; DL was reached in 2 min when ferrous ions were used, whereas it was achieved in 10 min under ferric ions.

The heterogeneous photo-Fenton processes at low concentrations of reagents (1 mg/L iron oxide and H_2O_2) were also found to be effective for MS2 bacteriophage inactivation, yielding total inactivation more slowly than its homogeneous counterpart, but still within minutes. Much like the two-faced ancient Roman god Janus, although NOM assisted the homogeneous photo-Fenton process, in its heterogeneous version organic matter acts as a catalyst poison, blocking iron oxides and competing with viral particles for sorption sites, thereby hindering the efficiency of the process. Nevertheless, as an inevitable constituent of natural waters, the effective observed MS2 bacteriophage titer reduction constitutes a highly positive result, indicating that the heterogeneous photo-Fenton process is robust and may eventually reach the necessary rates of inactivation.

The Fe(III)-based oxides (both maghemite and hematite) were the

most efficient in MS2 apparent inactivation rates after goethite, which is also ferric-based and the only iron-oxyhydroxide used in these experiments. The rate of inactivation by the heterogeneous photo-Fenton process followed the order of Goethite > Maghemite > Hematite > Wüstite > Natural iron > Magnetite. However, by applying surface normalization and cost-effectiveness, the order of efficiency of the system changed to Hematite > Maghemite > Magnetite > Goethite > Wüstite. Nanosized oxides were found to be less efficient than larger oxides, which exert higher oxidative action on small virus particles adsorbed on their surfaces.

Overall, the experimental results of this study provide insights into MS2 inactivation during the photo-Fenton process in natural waters, and this proposition summarizes the possible pathways involved that may exert said inactivation. This work has significance as a voluntary photo-Fenton application for drinking water purification purposes, as well as the environmental fate of the model virus used, showcasing the complexity of this issue. However, more work is necessary to elucidate the aspects of LMCT as well as the oxidative or reductive species generated under light. Finally, precipitated iron, colloidal particles, and other natural iron forms merit further consideration, as their role in natural waters is key to facilitating the photo-Fenton process.

Funding statement

The funding sources have been fully provided in the Acknowledgements section.

Ethics approval statement, patient consent statement, permission to reproduce material from other sources, or clinical trial registration

Not applicable.

CRediT authorship contribution statement

Farinelli Giulio: Investigation, Methodology, Writing – review & editing. **Garcia-Muñoz Patricia:** Writing – review & editing, Validation, Formal analysis, Data curation. **Pulgarin Cesar:** Writing – review & editing, Validation, Supervision, Resources, Project administration, Funding acquisition, Conceptualization. **Giannakis Stefanos:** Writing – review & editing, Validation, Supervision, Project administration, Methodology, Funding acquisition, Formal analysis, Conceptualization. **Oji-Okoro Ogadimma Cassandra:** Writing – original draft, Visualization, Methodology, Investigation. **Tian Na:** Writing – review & editing, Writing – original draft, Visualization, Software, Investigation, Formal analysis.

Declaration of Competing Interest

The authors declare that they have no known competing financial interests or personal relationships that could have appeared to influence the work reported in this paper.

Data Availability

Data will be made available on request.

Acknowledgments

This work was supported by the National Natural Science Foundation of China (Grant No. 42107102) and China Postdoctoral Science Foundation (No. 2020M672442). Na Tian would like to thank the China Scholarship Council for its financial support (CSC No. 202006415045). Stefanos Giannakis would like to acknowledge the REDDIS project, "Procesos reductivos como el Talón de Aquiles bacteriano en la desinfección de aguas residuales y en aguas naturales", which received funding from the Agencia Estatal de Investigación (Spain), "Proyectos Consolidación Investigadora 2022″ (CNS2022–135728). Last but not least, this Special Issue is dedicated to honoring the retirement of Prof. Santiago Esplugas at the Universitat de Barcelona (UB, Spain). Santi will be a key figure for researchers in Catalytic Advanced Oxidation Processes for a long time to come, with his great scientific achievements being surpassed only by his human qualities. His encouragement and wholehearted support were a key influence in the first scientific steps taken by Cesar Pulgarin The fortunate ones to meet him in person, will always remember his thought-provoking guidance and the way that a couple of his comments would give anyone food for scientific thought for a couple of months.

Appendix A. Supporting information

Supplementary data associated with this article can be found in the online version at doi:10.1016/j.cattod.2024.114536.

References

[1] P. Aldhous, Nature 422 (2003) 251.
[2] S.S. Sills, Water Res 33 (1999) 301–308.
[3] J. You, Y. Guo, R. Guo, X. Liu, Chem. Eng. J. 373 (2019) 624–641.
[4] M. Cho, J. Kim, J.Y. Kim, J. Yoon, J.H. Kim, Water Res. 44 (2010) 3410–3418.
[5] S.K. Loeb, W.C. Jennings, K.R. Wigginton, A.B. Boehm, Environ. Sci. Technol. 55 (2021) 8783–8792.
[6] S. Miller, Environ. Sci. Technol. 27 (1993) 2292–2294.
[7] K.G. McGuigan, R.M. Conroy, H.J. Mosler, M. du Preez, E. Ubomba-Jaswa, P. Fernandez-Ibanez, J. Hazard. Mater. 235-236 (2012) 29–46.
[8] S. Samoili, G. Farinelli, J.Á. Moreno-SanSegundo, K.G. McGuigan, J. Marugán, C. Pulgarín, S. Giannakis, Chem. Eng. J. 427 (2022) 130866.
[9] Z. Amiri, G. Moussavi, S. Mohammadi, S. Giannakis, J. Hazard. Mater. 408 (2021) 124634.
[10] D. Zhao, Curr. Pollut. Rep. (2015) 167–176.
[11] B. Halliwell, J. Neurochem 97 (2006) 1634–1658.
[12] I. Berruti, S. Nahim-Granados, M.J. Abeledo-Lameiro, I. Oller, M.I. Polo-Lopez, Molecules 26 (2021) 4890.
[13] Y.D. Chen, X.G. Duan, X. Zhou, R.P. Wang, S.B. Wang, N.Q. Ren, S.H. Ho, Chem. Eng. J. 409 (2021) 128207.
[14] L.C. Ferreira, M. Castro-Alférez, S. Nahim-Granados, M.I. Polo-López, M.S. Lucas, G. Li Puma, P. Fernández-Ibáñez, Chem. Eng. J. 381 (2020) 122275.
[15] M.A. Tony, P.J. Purcell, Y.Q. Zhao, A.M. Tayeb, M.F. El-Sherbiny, J. Environ. Sci. Heal. A 44 (2) (2009) 179–187.
[16] S. Papoustakis, Doctoral Thesis, EPFL (2015).
[17] S. Giannakis, S. Liu, A. Carratala, S. Rtimi, M. Talebi Amiri, M. Bensimon, C. Pulgarin, J. Hazard. Mater. 339 (2017) 223–231.
[18] W.G. Barb, J.H. Baxendale, P. George, K.R. Hargrave, Trans. Faraday Soc. 47 (1951) 591–616.
[19] J.J. Pignatello, Environ. Sci. Technol. 26 (1992) 944–951.
[20] J.J. Pignatello, E. Oliveros, A. MacKay, Crit. Rev. Environ. Sci. Tec. 36 (2006) 1–84.
[21] S. Pablo, M. Victoria, C. David, M. Yanko, H.D. Mansilla, J. Chil. Chem. Soc. 58 (2013) 2096–2101.
[22] S. Garda-Segura, E. Brillas, Water Res 45 (2011) 2975–2984.
[23] M. Roth, V. Jaquet, S. Lemeille, E.J. Bonetti, Y. Cambet, P. Francois, K.H. Krause, Antioxidants 11 (2022) 655.
[24] A. Rodriguez-Rojas, J.J. Kim, P.R. Johnston, O. Makarova, M. Eravci, C. Weise, R. Hengge, J. Rolff, PLoS Genet 16 (2020) 1008649.
[25] Y. Jin, Y. Shi, Z. Chen, R. Chen, X. Chen, X. Zheng, Y. Liu, R. Ding, Appl. Catal. B: Environ. 267 (2020) 118730.
[26] I.D.L.O. Jiménez, S. Giannakis, D. Grandjean, F. Breider, G. Grunauer, J.L. Casas López, J.A. Sánchez Pérez, C. Pulgarin, Appl. Catal. B: Environ. 263 (2020) 118158.
[27] L. Feng, C. Peillex-Delphe, C. Lu, D. Wang, S. Giannakis, C. Pulgarin, Water Res 182 (2020) 116049.
[28] M. Kohantorabi, S. Giannakis, M.R. Gholami, L. Feng, C. Pulgarin, Appl. Catal. B: Environ. 244 (2019) 983–995.
[29] A.G. Rincón, C. Pulgarin, Appl. Catal. B: Environ. 63 (2006) 222–231.
[30] S. Giannakis, M. Voumard, S. Rtimi, C. Pulgarin, Appl. Catal. B: Environ. 227 (2018) 285–295.
[31] A. Pulgarin, S. Giannakis, C. Pulgarin, C. Ludwig, D. Refardt, Appl. Catal. B: Environ. 265 (2020) 118615.
[32] P. Villegas- Guzman, S. Giannakis, S. Rtimi, D. Grandjean, M. Bensimon, L.F. de Alencastro, R. Torres-Palma, C. Pulgarin, Appl. Catal. B: Environ. 219 (2017) 538–549.
[33] J. Rodríguez-Chueca, S. Giannakis, M. Tranchant, P. Oulego, M. Bensimon, C. Pulgarín, Chem. Eng. J. 464 (2023) 142598.
[34] S. Giannakis, M.I.P. López, D. Spuhler, J.A.S. Pérez, P.F. Ibáñez, C. Pulgarin, Appl. Catal. B: Environ. 198 (2016) 431–446.
[35] K. Valegård, L. Liljas, K. Fridborg, T. Unge, Nature 345 (1990) 36–41.

[36] A.M. ElHadidy, S. Peldszus, M.I. Van Dyke, Sep. Purif. Technol. 120 (2013) 215–223.
[37] J.K. Choe, D.H. Richards, C.J. Wilson, W.A. Mitch, Environ. Sci. Technol. 49 (2015) 13331–13339.
[38] N. Dunkin, S. Weng, K.J. Schwab, J. McQuarrie, K. Bell, J.G. Jacangelo, Environ. Sci. Technol. 51 (2017) 2972–2981.
[39] K. Kim, J. Narayanan, A. Sen, S. Chellam, Environ. Sci. Technol. 55 (2021) 13198–13208.
[40] E. Ortega-Gómez, M.B. Martín, A. Carratalà, P.F. Ibañez, J.S. Pérez, C. Pulgarín, Appl. Catal. B: Environ. 174 (2015) 395–402.
[41] S. Giannakis, S. Liu, A. Carratalà, S. Rtimi, M. Bensimon, C. Pulgarin, Appl. Catal. B: Environ. 204 (2017) 156–166.
[42] Q.S. Meng, C.P. Gerba, Water Res 30 (1996) 2665–2668.
[43] J.Y. Kim, C. Lee, D.L. Sedlak, J. Yoon, K.L. Nelson, Water Res 44 (2010) 2647–2653.
[44] S.L. Rosado-Lausell, H. Wang, L. Gutiérrez, O.C. Romero-Maraccini, X.Z. Niu, K. Y. Gin, J.P. Croue, T.H. Nguyen, Water Res 47 (2013) 4869–4879.
[45] R.E. Pettit, CTI Res. (2012).
[46] B. Morgan, O. Lahav, Chemosphere 68 (2007) 2080–2084.
[47] J.I.Nieto Juarez, EPFL, (2012).
[48] J. Bartels, M.N. Souza, A. Schaper, P. Árki, S. Kroll, K. Rezwan, Environ. Sci. Technol. 50 (2016) 1973–1981.
[49] S.E. Beck, R.A. Rodriguez, M.A. Hawkins, T.M. Hargy, T.C. Larason, K.G. Linden, Appl. Environ. Microb. 82 (2016) 1468–1474.
[50] K.R. Wigginton, L. Menin, T. Sigstam, G. Gannon, M. Cascella, H.B. Hamidane, Y. O. Tsybin, P. Waridel, T. Kohn, Chembiochem 13 (2012) 837–845.
[51] B.M. Pecson, L. Decrey, T. Kohn, Water Res 46 (2012) 1763–1770.
[52] B. Yuan, M. Pham, T.H. Nguyen, Environ. Sci. Technol. 42 (2008) 7628–7633.
[53] S.S. Lin, M.D. Gurol, Environ. Sci. Technol. 32 (1998) 1417–1423.
[54] T. Kohn, K.L. Nelson, Environ. Sci. Technol. 41 (2007) 192–197.